




Research

Green synthesis of silver nanoparticles and their potential to enhance defense in cabbage crop against *Xanthomonas campestris* pv. *campestris*

Ivonaldo Reis Santos^{1,2}  · Fabiano Touzjian Pinheiro Kohlrausch Tavora¹  · Eduardo Andrade Franco Severo^{1,3} · Osmundo Brilhante Oliveira-Neto^{1,4}  · Angela Mehta¹  · Luciano Paulino Silva^{1,2} 

Received: 4 September 2024 / Accepted: 26 March 2025

Published online: 08 April 2025

© The Author(s) 2025 

Abstract

The green synthesis of metallic nanoparticles (MNPs) is a promising approach for plant disease management. In this study, eco-friendly nanoparticles were produced to fight black-rot disease of cruciferous crops caused by *Xanthomonas campestris* pv. *campestris* (Xcc). Silver nanoparticles (AgNPs) were synthesized by using aqueous extracts of cabbage (*Brassica oleracea* var. *capitata* L.), thale cress (*Arabidopsis thaliana* [L.] Heynh), neem (*Azadirachta indica* L.), and noni (*Morinda citrifolia* L.) leaves and fruit parts (peel and pulp/seeds), as reducing and stabilizing agents. The AgNPs syntheses were performed at six different concentrations of extracts in aqueous solutions of silver nitrate (AgNO_3), at 1 mmol L^{-1} . In total, 42 samples of AgNPs were produced, out of which, 14 were selected according to their hydrodynamic diameter (HD), polydispersity index (PDI), and Zeta potential (ZP) and further tested in vitro to evaluate their antibacterial activity against Xcc. The AgNPs with the highest antibacterial activity displayed the lowest HD ($192.3 \pm 1.1 \text{ nm}$) at $64 \mu\text{mol L}^{-1}$, particularly those synthesized using aqueous extract of noni fruit peel (AENFP) at 60 mg mL^{-1} . Furthermore, susceptible plants of cabbage were treated with AENFP- AgNPs, and the positive modulation of defense-related marker genes were captured by RT-qPCR. Plants treated with AENFP- AgNPs at $64 \mu\text{mol L}^{-1}$ when challenge with Xcc, showed a more tolerant phenotype, with leaves displaying reduced black rot symptoms up to 7 days post-infection. These results indicate that the application of AgNPs seems to trigger an effective defense response, probably due to the elicitor properties present in AgNPs synthesized from AENFP. The present study proposes an interesting alternative approach to control plant diseases.

Keywords AgNPs · Black-rot resistance · Green synthesis · Plant extracts · Plant priming-defense

Supplementary Information The online version contains supplementary material available at <https://doi.org/10.1007/s44372-025-00190-8>.

✉ Angela Mehta, angela.mehta@embrapa.br; ✉ Luciano Paulino Silva, luciano.paulino@embrapa.br | ¹Embrapa Recursos Genéticos e Biotecnologia, PBI, Av. W/5 Norte Final, Brasília, DF CEP 70770 - 917, Brazil. ²Programa de Pós-Graduação em Ciências Biológicas (Biologia Molecular), Universidade de Brasília, Instituto de Ciências Biológicas, Campus Universitário Darcy Ribeiro, Brasília, DF CEP 70910 - 900, Brazil. ³Universidade de Brasília, Instituto de Ciências Biológicas, Campus Universitário Darcy Ribeiro, Brasília, DF CEP 70910 - 900, Brazil. ⁴Departamento de Bioquímica e Biologia Molecular, Escola de Medicina, Centro Universitário Unieuro, SCE/SUL, Brasília, DF CEP 70200 - 001, Brazil.



1 Introduction

The *Brassicaceae* family comprises 338 genera and 3,709 species distributed worldwide [1]. The Brassica group has relevant socioeconomic impacts since it is used as edible vegetables, fodder for livestock, vegetable oils, biofuels, among other uses [2, 3]. The main Brassica vegetable crop cultivated is *Brassica oleracea* L., a highly important cruciferous vegetable that contains many nutrients and has a morphologically abundant variation. *B. oleracea* L. includes *B. oleracea* var. *capitata* (cabbage), *B. oleracea* var. *botrytis* (cauliflower), *B. oleracea* var. *italica* (broccolis), *B. oleracea* var. *gemmifera* (Brussels sprouts), and *B. oleracea* var. *acephala* (kale). Some varieties also have excellent ornamental properties. [4].

Cabbage is a popular vegetable, and its consumption is attractive due to its nutritional and antioxidant values [2, 3]. However, many diseases hinder cabbage production, reducing plant yield and nutritional value. One of these diseases, known as black rot, is caused by *Xanthomonas campestris* pv. *campestris* (Xcc), which is an important and potentially destructive bacteria, causing relevant economic losses and reducing both crop performance and quality [5–7]. Xcc is a Gram-negative bacterium that lives epiphytically on the leaf surface, and infects the plant through roots, stomata, hydathodes or wounds of the host plant, and colonizes the vascular system, invading the xylem and colonizing the mesophyll. Typical disease symptoms of black rot are V-shaped chlorosis on leaf edges with blackened veins, necrosis, and darkening of vascular tissues, which can lead to leaf fall and plant death [8, 9]. Xcc infection is particularly harmful due to biofilm formation, which contains degrading extracellular enzymes and other virulence factors [10]. The control of black rot disease has been only partially obtained by agronomical practices, such as, the use of Xcc-free planting material (i.e., seeds or seedlings), elimination of harvest residues from infected plants, and crop rotation, along with the extensive use of chemical agents which are potentially hazardous for human health and also to the environment [11]. In this context, the search for more efficient and sustainable strategies for the management of black rot disease is highly desired.

In the last few decades, several studies have demonstrated the use of metallic nanoparticles (MNPs) as a promising approach for plant disease management [12–14]. Thus, MNPs have achieved great importance in recent years because of their applicability in materials science, biology, medicine, chemistry and physics. There are several approaches to synthesize MNPs, such as physical and chemical synthesis, which are typically expensive, time-consuming, besides generating toxic substances that harm both the environment and human health [15, 16]. On the other hand, the biological synthesis or green synthesis is a method that has been increasingly used for the synthesis of MNPs, which consists of using reducing or stabilizing agents of low or zero toxicity, replacing conventional reagents that are toxic [17–19]. Therefore, the green synthesis of MNPs represents a more innovative and eco-friendly approach, in which different biological resources, such as fungi, bacteria, and plant extracts, are employed in the process [20]. This method is preferable to the chemical and physical approaches, particularly due to its non-toxic nature [21–23]. Several types of MNPs have been produced using green synthesis such as gold, copper, and silver. However, silver nanoparticles (AgNPs) have proven to be the most convenient due to their broad spectrum applications in food, health and industry [24–26]. AgNPs have several interesting unique properties, such as catalytic activity, conductivity, stability and antimicrobial activity [27, 28].

In this context, the present study aimed to produce eco-friendly AgNPs to combat black-rot disease caused by Xcc using aqueous extracts from various plant sources. Leaves from cabbage (*B. oleracea* var. *capitata* L.), thale cress (*Arabidopsis thaliana* [L.] Heynh), and the tropical plants neem (*Azadirachta indica* L.) and noni (*Morinda citrifolia* L.), as well as from noni fruit parts, including peel and pulp/seeds, were used as reducing and stabilizing agents in the green synthesis of AgNPs.

2 Materials and methods

2.1 Plant material and aqueous extracts preparation

For this study, leaves of cabbage (*B. oleracea* var. *capitata*), thale cress (*A. thaliana*), neem (*A. indica*), and noni (*M. citrifolia*), as well as noni fruits, were used in the formulation of aqueous extracts by decoction. Healthy plants of *B. oleracea* var. *capitata* (50 days old), *A. thaliana* (90 days old), and *A. indica* were cultivated and collected at Embrapa

Genetic Resources and Biotechnology, Brasília, DF, Brazil. *A. indica* leaves and *M. citrifolia* leaves and fruits were obtained from Sobradinho (administrative precinct of Brasília/DF), located at DF 150 km 11 Rua do Mato, Chácara 15 Fercal. The leaves were thoroughly washed three times in sterile distilled water, ground in liquid nitrogen, weighed, and sampled separately in glass beakers. For the production of noni fruit extracts, ripe fruits were firstly washed with 0.1% Extran® (Merck Millipore™, USA) neutral detergent, and then with sterile distilled water. Fruit peel was carefully removed using a scalpel, and both the peel and fruit pulp/seeds underwent the same steps as plant leaves. Next, 0.5 g of all samples were boiled separately in 1 mL of deionized water using a hot plate for 3 min according to Santiago et al. [29], with modifications. The material was filtered by gravity filtration through Qualy No. 7 (14 µm pore) filter paper (Qualy Comercial Eireli, Passos, MG, Brazil) and stored in 15 mL polypropylene tubes at 4 °C for further use in the green synthesis of AgNPs. A total of 7 samples of aqueous extracts were obtained.

2.2 Green synthesis and characterization of silver nanoparticles (AgNPs)

AgNPs were synthesized by using 1 mmol L⁻¹ of aqueous solution of silver nitrate (AgNO₃) along with different concentrations (i.e., 10, 15, 20, 25, 30, and 60 mg mL⁻¹) of aqueous extract of leaves from noni (AELN), neem (collected at Sobradinho) (AELNES), neem (collected at Brasília) (AELNEB), cabbage (AELC), and *A. thaliana* (AELA), and aqueous extract of noni fruits (peel or pulp/seed) (AENFP or AENFPS), totalizing 42 samples (SupplementaryTable 1). For the control samples, AgNO₃ solution was replaced by sterile ultrapure water. The reactions involving AELN, AELNES, AELNEB, AELC, AELA, AENFP, and AENFPS aqueous extracts, aimed at converting Ag⁺ ions into Ag⁰, were incubated at 75 °C, in the dark for 2.5 h. The kinetic effects of all reactions were monitored using a Glomax® microplate reader (Promega™, USA), at room temperature. The light absorbance (optical density) of samples was measured at 450, 490, and 630 nm, with 30 min intervals, for 2.5 h. All measurements were performed in triplicates on 96-well microplates in a final volume of 100 µL per well. Dynamic light scattering (DLS) was subsequently employed to characterize the physical properties of the synthesized AgNPs, including the hydrodynamic diameter (HD), polydispersity index (PDI), and Zeta potential (ZP), using a ZetaSizer Nano ZS® (Malvern, UK) equipped with a 4 mW He–Ne laser operating at 633 nm and a detection angle of 173. AgNPs suspensions were diluted in ultrapure water 10 × (v/v) and 3 measurements were performed. ZetaSizer® V.7 software was used to analyze HD, PDI, and ZP parameters. Finally, all AgNPs suspensions were stored at 4 °C until further use. Statistical analyses were conducted using one-way analysis of variance (ANOVA) test followed by the least significant difference mean comparison test (at $P = 0.05$) using the program PAST. A total of 2 µL of AgNPs synthesized with 60 mg mL⁻¹ of AENFP (at 64 µmol L⁻¹) diluted 10 × in type I water were deposited onto freshly-cleaved muscovite mica surface and allowed to air dry in a controlled environment. The sample was then mounted on a metallic sample holder using double-sided adhesive tape, which was secured at the base of the equipment. The analyses were performed in ambient air at approximately 22 °C using an atomic force microscope (Shimadzu SPM- 9600, Japan), equipped with a scanner that has a maximum scanning area of 125 × 125 µm². Dynamic phase mode was employed with a rectangular cantilever, featuring a conical silicon tip with a spring constant of about 42 N/m, a resonance frequency of about 300 kHz, and a sweep frequency of 1 Hz. Imaging was performed over 10 µm × 10 µm areas, with a resolution of 512 × 512 lines and further digitally zoomed to 5 µm × 5 µm areas. Images were processed for plane correction and individual segmentation using the instrument's dedicated offline software.

2.3 In vitro antibacterial activity assay against *Xanthomonas campestris* pv. *campestris*

Greenly synthesized AgNPs were tested for potential antibacterial activity against *Xcc* by evaluating the minimum inhibitory concentration (MIC) of each AgNP-suspension, according to Santiago et al. [29] with modifications. Based on the physicochemical characterization results, AgNPs suspensions showing the highest and lowest HD, PDI, and ZP values of each group were selected: AELN-AgNPs (10 or 60 mg mL⁻¹), AELNES-AgNPs (10 or 60 mg mL⁻¹), AELNEB-AgNPs (10 or 20 mg mL⁻¹), AELC-AgNPs (25 or 60 mg mL⁻¹), AELA-AgNPs (10 or 60 mg mL⁻¹), AENFP-AgNPs (25 or 60 mg mL⁻¹) and AENFPS-AgNPs (15 or 60 mg mL⁻¹), totalizing 14 samples. *Xcc* was grown at 28 °C in nutrient-yeast extract-glycerol (NYG) medium (3 g/L yeast extract, 5 g/L peptone, 20 g/L glycerol, pH 7.0). For solid media, agar was added at a concentration of 1.5% (w/vol). After 72 h, bacterial cells were pre-cultured in liquid NYG medium for 16 h and the optical density (OD) was adjusted to A₆₀₀ = 0.050, using a spectrophotometer. Next, 85 µL of the bacterial suspension was added to the green-synthesized AgNP or control samples. The positive control used was AgNO₃ at final concentrations of 8, 16, 32, 64, 128, and 256 µmol L⁻¹, while the negative control consisted of sterile ultrapure water, in a final volume of 100 µL.

The assay was performed in a 96-well microplate, which was incubated at 28 °C for 72 h, and the MIC was determined by visual inspection.

2.4 Treatment of *B. oleracea* with AgNPs for analysis of defense-related genes by RT-qPCR

Green synthesized AgNPs were tested for their potential to trigger plant defense by analyzing the expression of defense-related biomarker genes in cabbage crops. AgNPs synthesized with 60 mg mL⁻¹ of AENFP (at 64 µmol L⁻¹), which displayed the highest antibacterial activity, and the plant cultivar Veloce (a genotype of *B. oleracea* var. *capitata*, susceptible to black rot disease) were used in this assay. Plant seeds were disinfested by soaking in 70% ethanol for 1 min, 3% sodium hypochlorite for 15 min, and finally washed 5× with sterile distilled water. Further, seeds were sown in plastic pots containing a mixture of sterile soil, manure, and sterile sand (3:1:1 w/w/w) and cultivated in greenhouse at Embrapa Genetic Resources and Biotechnology, Brasília/DF. Each plastic pot contained one plant, and three plants constituted each sample. Three biological replicates (samples) were used, totaling 27 plants. At 18 days after germination, plants had their leaves (adaxial surface) sprayed with 1 mL of selected AENFP-AgNPs (64 µmol L⁻¹) or AgNO₃ solution (64 µmol L⁻¹). Plants in the control group had no treatment. Sample leaves were collected 24 h post-treatment, ground in liquid nitrogen, and stored at – 80 °C until further use.

2.5 RNA isolation and cDNA synthesis

Plant RNA isolation was performed using Trizol[®] method (Invitrogen[™], USA), according to the manufacturer's instructions, and then quantified by using NanoDrop[®] spectrophotometer (ND- 1000 UV-Vis, ThermoFisher[™], USA). To verify the integrity of the isolated RNA, the samples were analyzed in a denaturing agarose gel (1% agarose; 1× TAE Buffer), pre-stained with ethidium bromide (0.5 mg mL⁻¹) [30]. To remove potential genomic DNA contamination, the Turbo[®] DNase enzyme (Ambion[™], USA) was applied to the RNA samples. cDNA synthesis was performed using 2 µg of treated RNA using GoScript[®] Reverse Transcription System (Promega[™], USA), and stored at – 20 °C.

2.6 Primer design, RT-qPCR and data analysis

Genes previously described in the literature with possible involvement in defense response were selected [31] Table 1. Primer3 Plus software [32] was used to design all primers, and the absence of amplification and non-specific products were evaluated using the software OligoAnalyzer 3.1 [33]. The primers were designed with an average temperature of 57–63 °C and length of 20 nucleotides. RT-qPCR analyses were performed according to Santos et al. [34], in 96-well microplates in a 7300[™] 96-well Real-Time PCR Systems thermal cycler (Applied Biosystems[™], USA), using SYBR[™] Green detection system, according to the manufacturer's instructions. All reactions were performed in a total volume of 10 µL composed of 5 µL of Fast SYBR[®] Green Master Mix (Applied Biosystems[™], USA), 0.2 µL of each primer at an initial concentration of 10 µmol L⁻¹ (forward and reverse), and 2 µL of single-stranded cDNA (20-fold diluted) corresponding to each sample to be analyzed. The PCR program consisted of one first step at 95 °C for 10 min to activate the Taq polymerase enzyme ("hot start") and 40 cycles at 95 °C for 15 s, 60 °C for 60 s. To verify the presence of primer dimers and non-specific products, the denaturation curve—"melting curve" was analyzed after the end of the amplification. The program was 95 °C for 15 s, 60 °C for 60 s, increasing 0.3 °C each cycle until reaching 95 °C. Raw fluorescence data from all runs were imported into Real-time PCR Miner software [35], to determine PCR efficiency and Cq value. Gene expression analysis was conducted using the Rest software [36], which enables group-wise comparisons and statistical evaluation of relative expression levels. Normalization was performed using internal reference genes: Ubiquitin- 60S ribosomal protein L40/XP_013634027.1 (*UBI*) and TATA-box-binding protein 1/XP_013583944.1 (*TBP*), known as constitutive genes [37]. To compare differences in expression between groups, the t-test was used with 4 degrees of freedom, n = 9 (3 biological and 3 technical replicates for each sample).

2.7 Pathogenicity assay in AgNPs-treated plants

To verify the potential of AENFP-AgNPs to reduce the symptoms of black rot disease in *B. oleracea* var. *capitata* Veloce (susceptible to Xcc isolate 51), the seeds were subjected to disinfestations with 3% sodium hypochlorite and placed to germinate in plastic cups of 200 mL containing a mixture of sterile soil, manure, and sterile sand (3:1:1 w/w/w). A total of 3 biological replicates were used, totaling 9 plants. To evaluate disease symptoms, at 18 days after germination, the

Table 1 General information of selected targets for gene expression analysis

Gene	Access GenBank	Annotation/Gene name	Forward primer (5'-3')	TM (°C)	Reverse primer (5'-3')	TM (°C)	Amplicon	Primer efficiency (%)
<i>FADS</i>	XM_002302577.2	XP_002302613.1/Fatty acid desaturase/cytochrome b5 fusion protein	ATAACAGAAATCGCGCAGCTC	53	TGAAGAACTTGGTGAGACG	52	162	87
<i>CYP83B1</i>	NM_119299.3	NP_194878.1/Cytochrome P450	CTTAGACTTCACCCCAACCAT	49	CTCTCGGGACAAAACCTCG	50	167	85
<i>DEFL</i>	NM_001036559.3	NP_001031636.2/Defensin-like family protein	ATCAGCAATGTCTGGTGCGAG	53	TTGTCTAGGGATGGGTCCAG	52	179	86
<i>SAPX</i>	NM_001340582.1	NP_001319883.1/Stromal ascorbate peroxidase	TTCCTCTCTTCGCACTCAAG	52	GAAACTCCGATTACACCAACG	52	166	88
<i>DAO</i>	XM_013745193.1	XP_013600647.1/2-oxoglutarate-dependent dioxygenase DAO-like	CAAATCTCTCCCAAAACACAG	51	CCCTTGGAGCAATCAATCTC	50	160	86
<i>SRG2</i>	NM_001247299.2	XP_001234228.2/Salt responsive protein 2	ACGAGGAAAACGGAGACATC	52	TTAACCATAACCGCTCTG	52	166	88
<i>PIDRP8</i>	XM_008345553.1	XP_008343775.1/Pathogen-induced defense-responsive protein 8	AGTCTTGCAITGGACCCAAAC	60	TCTACAATCGCGTCTTCAG	60	173	88
<i>ARP</i>	XM_006371764.1	XP_006371826.1/Avirulence-responsive family protein	TAACAGATGCTCAGCTAGAG	49	CGAAATCCCATTCTCCAT	45	162	83
<i>UBJ*</i>	XM_013778573.1	XP_013634027.1/Ubiquitin-60S ribosomal protein L40	ATGTCAAGGCCCAAGATCCAG	52	GAGCCAAAGCCCATCAAGAG	51	186	86
<i>TBP*</i>	XM_013728490.1	XP_013583944.1/TATA-box-binding protein 1	TCTTGCTCCAGTACAAACC	52	ACATTGTGTCGACGGTGAAC	53	177	87

* Reference genes

plants were sprayed on the adaxial face of the leaves with 1 mL of AENFP-AgNPs synthesized with 60 mg mL⁻¹ of AENFP at a concentration of 64 µmol L⁻¹, or AgNO₃ (64 µmol L⁻¹) or without treatment (control condition). At 24 h after the application of the treatments, plants were sprayed with Xcc isolate 51. The bacterium was grown in NYG liquid medium for 24 h, centrifuged and suspended in water. Approximately 1 mL of the bacterial suspension ($A_{600} = 0.300$) was sprayed on the leaves of all plants. The inoculated plants were maintained in a Greenhouse and disease symptoms were visually monitored and quantified. The percentage of damaged leaf area was captured from 3 leaves per plant ($n = 9$), at three time points (5, 7 and 10 days after inoculation—dai), using the software QUANT[®] [38]. One-way ANOVA and post hoc two-sample t-test were performed for significance ($p < 0.05$).

3 Results and discussion

3.1 UV–Vis spectroscopy analysis of AgNPs generation process

The green synthesis routes employing AELN, AELNES, AELNEB, AELC, AELA, AENFP, and AENFPS resulted in AgNPs with distinct physicochemical properties suitable for diverse applications, including the control of Xcc in Brassica crops. The green synthesis approach is simple and eco-friendly and can be extended to the preparation of other types of MNPs such as copper nanoparticles, with a wide range of applications in the field of materials sciences, as well as in agriculture.

The monitoring of AgNPs synthesis reactions by spectrophotometry is an important step in the AgNPs formation process. According to Baker et al. [39], AgNPs formed after green synthesis exhibit a surface plasmon resonance (SPR) that gives rise to characteristic peaks in absorptions in the electromagnetic spectrum. The green routes-based synthesis of all AgNPs used in this study was monitored and confirmed by performing UV–Vis spectral analysis. An increase in the aqueous extract concentration (from 10 to 60 mg mL⁻¹) was directly correlated with enhanced color intensity of the AELNES, AELNEB, AELC, AELA, AENFP, and AENFPS suspensions. In contrast, higher concentrations of AELN resulted in diminished color intensity.

Green synthesis of nanoparticles was confirmed by a color change in the mixture of AgNO₃ and plant extract (Fig. 1). The synthesis of nanoparticles is directly proportional to the availability of reducing and capping agents in the plant extract. The availability of the capping agents decreases as reaction time increases, resulting in the stabilization and capping of nanoparticles [40]. This visual observation was validated by quantifying the suspension light absorbance (at 490 nm wavelength) every 30 min for 2.5 h (Fig. 2). Such phenomena are supported by Alsammarraie et al. [41], whose work involving green synthesis of AgNPs has demonstrated that aqueous extracts of turmeric (*Curcuma longa* L.) plant roots change suspensions color from yellow to dark reddish brown due to the reduction of silver ions (Ag⁺) by redox-active organic biomolecules to form AgNPs. The color changes in AgNPs samples are due to the presence of plant extract components such as polyphenols (terpenoids, flavonoids, tannins), proteins (enzymes), organic acids and alkaloids that

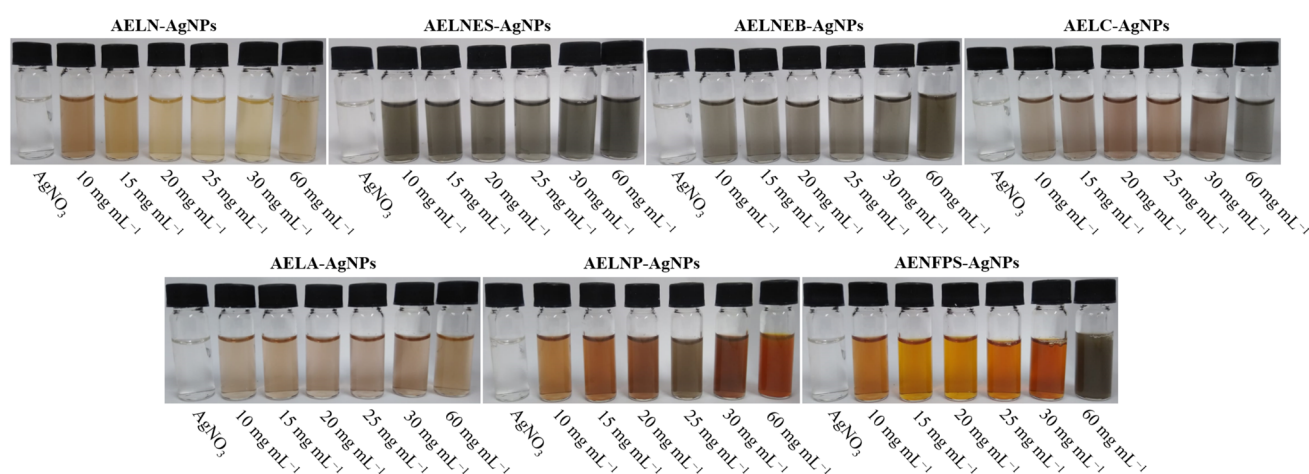


Fig. 1 Visual appearance of all greenly-synthesized AgNPs suspensions using 1 mmol L⁻¹ of silver nitrate (AgNO₃) along with six different concentrations (10, 15, 20, 25, 30, and 60 mg mL⁻¹) of aqueous extracts from cabbage (AELC), thale cress (AELA), noni (AELN), and neem plant leaves, as well as aqueous extract of noni peel (AENFP) and pulp/seed fruit parts (AENFPS), after 2.5 h of reaction. AgNO₃ translucent suspension (1 mmol L⁻¹) represents the control condition

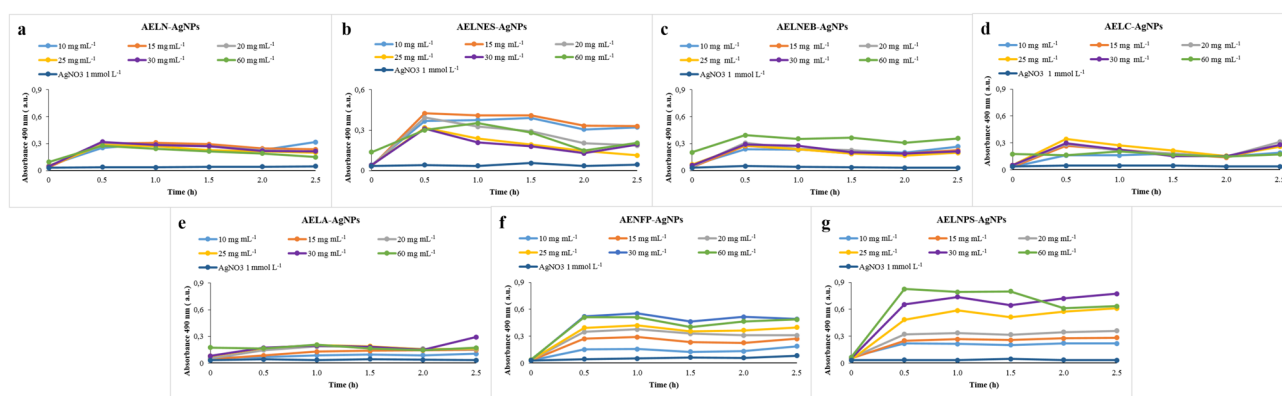


Fig. 2 Kinetic curves of AgNPs synthesis reactions characterized by UV-Vis spectroscopy. **A–G** AELN-AgNPs, AELNES-AgNPs, AELNEB-AgNPs, AELC-AgNPs, AELA-AgNPs, AENFP-AgNPs, and AENFPS-AgNPs suspensions, respectively. Different color curves ($n = 7$) represent all six different concentrations (10, 15, 20, 25, 30, and 60 mg mL^{-1}) of aqueous extract used in suspension syntheses, and the control condition (1 mmol L^{-1} of AgNO_3 , dark blue curve). Suspension light absorbance was measured at 490 nm (wavelength) at six time points (0, 0.5, 1.0, 1.5, 2.0, and 2.5 h) during the reactions

act as reducing and stabilizing agents. Several similar studies have been performed using plant extracts for the synthesis of AgNPs [29, 42], showing the high potential of these NPs for several biotechnological applications.

3.2 Assessment of AgNPs physicochemical properties by dynamic light scattering (DLS) and atomic force microscopy (AFM)

Dynamic light scattering (DLS) analysis confirmed the formation of the AgNPs and provided insights into the size and stability of the particles. The AELN-AgNPs, AELNES-AgNPs, AELNEB-AgNPs, AELC-AgNPs, AELA-AgNPs, AENFP-AgNPs and AENFPS-AgNPs showed variation in hydrodynamic diameters (HD) and polydispersity indexes (PDI) depending on the extract concentrations. In the AELC-AgNPs suspension, the HD ranged from 2136.0 to 3218.0 nm, and PDI 0.481–0.709, and in the AELA-AgNPs the HD ranged from 266.6 to 4636.0 nm and PDI 0.372–0.646. In the AELNEB-AgNPs and AELNES-AgNPs suspensions, the HD ranged from 890.1 to 2958.0 and 168.3–1513.0 nm, and presented PDI values of 0.506–0.780 and 0.371–0.717, respectively. In the AELN-AgNPs suspension, the HD ranged from 724.0 to 1652.0 nm, and showed moderate PDI (0.415–0.543). In the AENFP-AgNPs and AENFPS-AgNPs suspensions, the HD

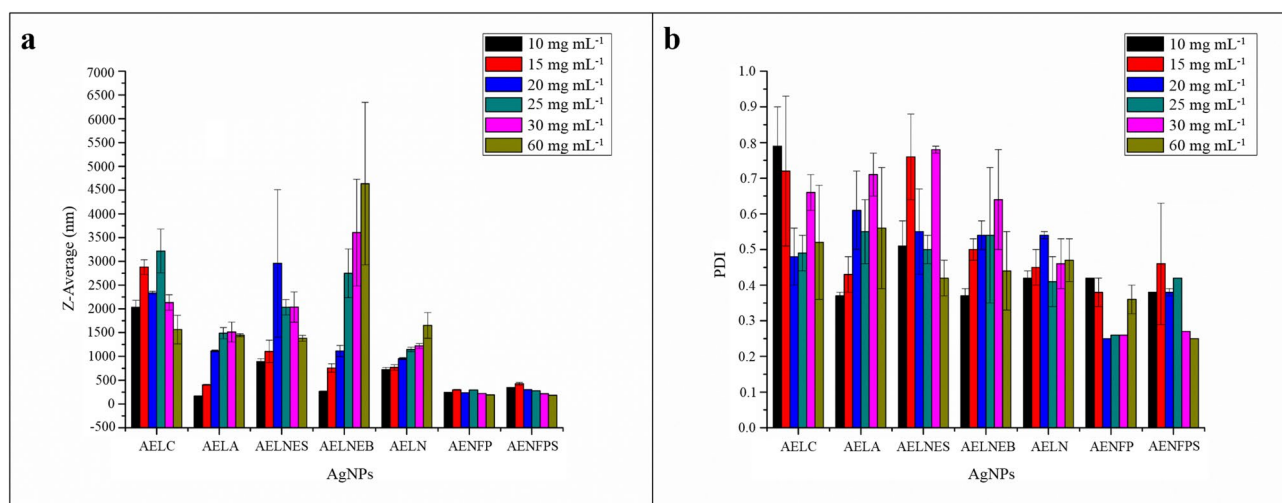


Fig. 3 Physicochemical parameters of AgNPs. **a** Hydrodynamic diameter (Z-Average) and **b** Polydispersity Index (PDI) of all greenly-synthesized AgNPs suspensions using 1 mmol L^{-1} of silver nitrate (AgNO_3) along with six different concentrations (10, 15, 20, 25, 30, and 60 mg mL^{-1}) of aqueous extract obtained from cabbage (AELC), thale cress (AELA), noni (AELN), and neem plant leaves, as well as aqueous extract of noni peel (AENFP) and pulp/seed fruit parts (AENFPS)

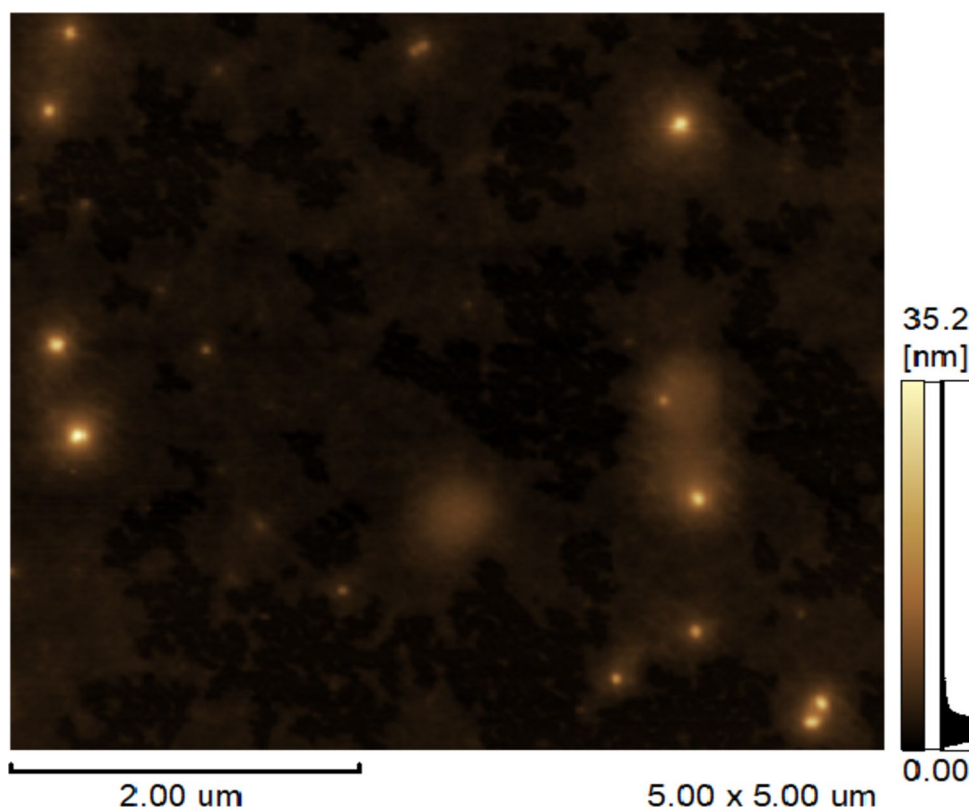
ranged from 184.7 to 422.8 and PDI 0.255–0.466. The Zeta potential of all these AgNPs ranged from – 11.2 to – 23.7 mV (Supplementary Table 2, Fig. 3).

The characterization of the AgNPs by DLS, in relation to the size of the particles, provided the HD of the AgNPs with variation between 168.3 nm and 4636.0 nm approximately. HD is related to particle size in water, an important parameter that can affect biodistribution properties of suspensions. In Fig. 3a it can be observed that the samples of AgNPs obtained by synthesis with AENFP and AENFPS presented nanoparticles with moderate PDI when compared to particles synthesized with AELN, AELNES, AELNEB, AELC and AELA. PDI quantifies the distribution width of particle sizes, serving as an indicator of suspension homogeneity. In this study, it was overall below 0.500 (in average) for all nanosuspensions, which indicates a relatively uniform particle size distribution despite not being monodisperse. According to Fig. 3a, it can be observed that the increases in the concentrations of AELNEB, AELN and AELA resulted in an increase trend in the values of HD. On the other hand, increasing concentrations of AELNES, AELC, AENFP and AENFPS showed inverse effects on the trend of both HD physical properties. The results also showed that the increases in the concentrations of AENFP and AENFPS resulted in a decrease trend in the values of PDI, ultimately reflecting a greater homogeneity of AgNP sizes (Fig. 3a). Indeed, the present study showed that the increasing concentrations influenced the size and PDI of the AgNPs.

Although DLS is the ultimate technique aiming at the determination of HD of AgNPs in colloidal suspensions, the use of high resolution microscopic techniques is mandatory when investigating the shape of nanoparticles. AFM height images of AgNPs synthesized with 60 mg mL⁻¹ of AENFP (at 64 µmol L⁻¹) showed spherical nanoparticles surrounded by amorphous materials probably from AENFP (Fig. 4).

The Zeta potential value, which reflects the surface properties of nanomaterials is another important measure that can be used to indicate well-stabilized nanosuspensions. The AgNP sample with the lowest concentration of extract (10 mg mL⁻¹) was obtained from noni leaves, presenting the most negative surface charge among all the AgNPs samples, with approximately – 23.7 mV. This feature provided a greater colloidal stability when compared to the other samples, which may be related to the possibility of phytochemical differences present in this species [43, 44].

Fig. 4 Atomic force microscopy top-view height image acquired in dynamic-phase mode of AgNPs synthesized with 60 mg mL⁻¹ of AENFP (at 64 µmol L⁻¹)



3.3 AgNPs negatively affect the survival of *X. campestris* pv. *campestris* in vitro

Several studies reported that Gram-positive bacteria are more resistant to the mechanisms of action of AgNPs [45, 46], primarily due to their thicker peptidoglycan layer (spanning 80 nm) with covalently bound teichoic and teicuronic acids, compared to Gram-negative bacteria. Conversely, Gram-negative bacteria possess a thinner layer of lipopolysaccharides (1–3 μm thick) and peptidoglycans (~ 8 nm thick), making them more permeable to AgNP-derived ions. This arrangement can facilitate the entry of AgNP-derived ions and therefore more susceptible to AgNP exposition [47]. The physical interaction between AgNPs and bacterial cell wall results in more pronounced destruction in Gram-negative bacteria, as they lack the thick peptidoglycan layer that acts as a protective barrier in Gram-positive bacteria.

Based on the physicochemical features of the AgNPs, the 14 most promising suspensions were selected (7 aqueous extracts at two different concentrations each) to assess their in vitro antibacterial activity against *Xcc* (Table 2). The results demonstrated that AELN-AgNPs (10 mg mL⁻¹) exhibited a lower HD value (724.0 \pm 45.2 nm) and higher antibacterial activity at a final concentration of 128 $\mu\text{mol L}^{-1}$ (Table 1). On the other hand, AENFP-AgNPs, when synthesized with the higher concentration of AENFP (60 mg mL⁻¹), presented the lowest HD value (192.3 \pm 1.1 nm) and exhibited the highest antibacterial activity against *Xcc*51 at a concentration of 64 $\mu\text{mol L}^{-1}$, ultimately standing out as the most promising candidate suspension to control the causal agent of black rot disease. Five out of 14 suspensions (36% of the total suspensions) did not exhibit any antibacterial activity (considering *Xcc*51 growth impairment in vitro) at the maximum concentration evaluated (256 $\mu\text{mol L}^{-1}$). The results from the minimal inhibitory concentration (MIC) in vitro assay suggested that antibacterial activity of the green-synthesized AgNPs is not solely associated with the increase of aqueous extract concentration in the reaction, but even more with a lower Z-average (HD) of the AgNPs.

The results obtained in this study indicate that AENFP-AgNPs synthesized with 60 mg mL⁻¹ at a concentration of 64 $\mu\text{mol L}^{-1}$ (equivalent to AgNO₃) appear to be effective in controlling *Xcc*, acting as a bactericidal or bacteriostatic agent. In general, the antibacterial activity of AgNPs synthesized using AELN, AELNES, AELNEB, AELA, AENFP, and AENFPS may

Table 2 Minimal inhibitory concentration (MIC) in vitro assay to evaluate potential antibacterial activity of the most promising green-based AgNPs formulations against *X. campestris* pv. *campestris*

AELN	Z-Average (nm)	Pdl	Zeta potential (mV)	MIC ($\mu\text{mol L}^{-1}$)
AELN-AgNPs_10 mg mL ⁻¹	724.0 \pm 45.17	0.423 \pm 0.020	- 23.7 \pm 0.15	128
AELN-AgNPs_60 mg mL ⁻¹	1652.0 \pm 270.3	0.474 \pm 0.065	- 17.0 \pm 0.45	256
AELNES	Z-Average (nm)	Pdl	Zeta potential (mV)	MIC ($\mu\text{mol L}^{-1}$)
AELNES-AgNPs_10 mg mL ⁻¹	168.3 \pm 2.93	0.371 \pm 0.012	- 21.6 \pm 0.47	256
AELNES-AgNPs_60 mg mL ⁻¹	1513.0 \pm 207.9	0.717 \pm 0.065	- 20.4 \pm 0.47	-
AELNEB	Z-Average (nm)	Pdl	Zeta potential (mV)	MIC ($\mu\text{mol L}^{-1}$)
AELNEB-AgNPs_10 mg mL ⁻¹	890.1 \pm 63.28	0.519 \pm 0.071	- 18.2 \pm 0.41	256
AELNEB-AgNPs_20 mg mL ⁻¹	2958.0 \pm 1549.0	0.558 \pm 0.124	- 13.9 \pm 1.30	-
AELC	Z-Average (nm)	Pdl	Zeta potential (mV)	MIC ($\mu\text{mol L}^{-1}$)
AELC-AgNPs_25 mg mL ⁻¹	3218.0 \pm 461.1	0.497 \pm 0.054	- 19.5 \pm 1.67	-
AELC-AgNPs_60 mg mL ⁻¹	1566.0 \pm 300.2	0.524 \pm 0.160	- 17.0 \pm 1.57	-
AELA	Z-Average (nm)	Pdl	Zeta potential (mV)	MIC ($\mu\text{mol L}^{-1}$)
AELA-AgNPs_10 mg mL ⁻¹	266.6 \pm 6.57	0.372 \pm 0.021	- 16.5 \pm 2.97	128
AELA-AgNPs_60 mg mL ⁻¹	4636.0 \pm 1708.0	0.443 \pm 0.110	- 11.2 \pm 1.17	128
AENFP	Z-Average (nm)	Pdl	Zeta potential (mV)	MIC ($\mu\text{mol L}^{-1}$)
AENFP-AgNPs_25 mg mL ⁻¹	293.4 \pm 4.59	0.268 \pm 0.002	- 23.4 \pm 0.11	128
AENFP-AgNPs_60 mg mL ⁻¹	192.3 \pm 1.06	0.362 \pm 0.047	- 19.6 \pm 1.83	64
AENFPS	Z-Average (nm)	Pdl	Zeta potential (mV)	MIC ($\mu\text{mol L}^{-1}$)
AENFPS-AgNPs_15 mg mL ⁻¹	422.8 \pm 30.28	0.466 \pm 0.171	- 18.4 \pm 1.88	128
AENFPS-AgNPs_60 mg mL ⁻¹	184.1 \pm 2.66	0.278 \pm 0.004	- 16.2 \pm 0.36	-
AgNO ₃	Z-Average (nm)	Pdl	Zeta potential (mV)	MIC ($\mu\text{mol L}^{-1}$)
Ag +	-	-	-	64

The bacterial isolate *Xcc*51 was incubated with seven nanoformulations synthesized with two different concentration of aqueous extract each (n = 14 samples) at a final AgNPs concentrations of 8, 16, 32, 64, 128, and 256 $\mu\text{mol L}^{-1}$. In the control samples, aqueous extracts were replaced by sterile ultrapure water. The assay was performed in a 96-well microplate incubated at 28 °C for 72 h, when the MIC was evaluated

be attributed to the binding between the bacterial cell wall and the AgNPs. This binding leads to the accumulation of membrane protein precursors, which leads to protein disruption, loss of proton motivating force, and, ultimately, cell death [41]. Furthermore, an array of evidence have linked the small dimensions of AgNPs to enhanced antibacterial activity [48–50], a fact that can be explained by the size vs surface area concept. For instance, smaller AgNPs have a faster rate of silver ion (Ag^+) release due to their larger surface area to volume ratio, thereby showing a greater toxicity as compared to larger AgNPs. This can increase the production of reactive oxygen species (ROS), which consequently can damage and inactivate biomolecules like lipids, DNA, and proteins [51].

Several studies have been conducted using plant extracts as reducing and stabilizing agents for the synthesis of AgNPs, including extracts of blackberry (*Morus alba*), pineapple (*Ananas comosus*), neem (*A. indica*), peach (*Prunus persica*), aztec fennel (*Phylla dulcis*), Black cumin (*Nigella sativa*), Flamboyant (*Delonix regia* var. *flavida*, Fabaceae), *Handroanthus heptaphyllus* (Vell.) Mattos, tomato (*Solanum lycopersicum*) and black cumin (*Nigella sativa*), which also exhibited remarkable antibacterial activity [29, 42, 52–58]. AgNPs can interact with proteins and phospholipids that are linked to bacterial membrane proton pumps, which results in membrane disruption, cell metabolism alteration, and cell death [59]. According to Lee et al. [60], the antimicrobial activity of AgNPs depends mainly on two variables, the concentration of silver ions and the sensitivity of each microbial species to silver.

Nevertheless, several studies reported that AgNPs with larger dimensions also have notable biological activity, indicating that nanoparticles toxicity is associated with other factors beyond its size, such as shape, concentration, capping agents, and colloidal state of AgNPs [61, 62]. Other factors that may be important in the mechanism of action of AgNPs include the formulation process, the environment, the bacterial defense mechanism and the physical characteristics. Our results are very consistent with those from literature, pointing to the optimal features of our green synthesis-based approach aiming at the formation of AgNPs and their substantial activity against *Xcc*.

3.4 AENFP-AgNPs induced positive modulation of immunity-related biomarker genes in *B. oleracea*

To reduce the severity of diseases, the induction of systemic resistance in the host plant has become a goal of paramount importance, as it is low cost and does not cause adverse effects on the environment or human health [63, 64]. Several nanomaterials can be used as plant defense elicitors, such as silver, titanium, and copper nanoparticles, which enhance antimicrobial activity against phytopathogens [65–67]. One of the most recent alternatives to control phytopathogens is the use of AgNPs [68–70]. AgNPs exhibit broad-spectrum antimicrobial activity, but the action mechanisms underlying their action in the plant defense response remain to be clarified.

In this study, qRT-PCR was used to analyze the relative expression of 8 defense-related biomarker genes in Brassica plants treated with a suspension of AENFP-AgNPs synthesized with 60 mg mL^{-1} of AENFP, which exhibited the highest antibacterial effects in in vitro assays. Plants were treated with either the AENFP-AgNPs suspension, an aqueous solution of AgNO_3 at a final concentration of $64 \mu\text{mol L}^{-1}$, or left untreated (control condition). The results showed that five out of eight (62.5%) analyzed genes displayed modulated expression following AgNPs treatment (Fig. 5a). The

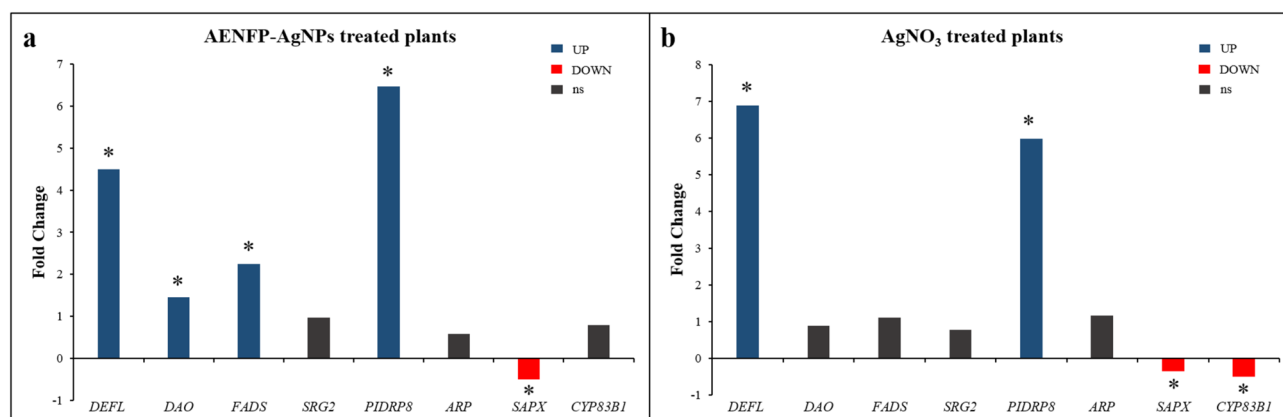


Fig. 5 Relative expression analysis of targeted genes associated with plant defense response. **a** Foliar treatment with AENFP-AgNPs synthesized with 60 mg mL^{-1} of AENFP at a concentration of $64 \mu\text{mol L}^{-1}$ of silver nitrate (AgNO_3) solution; **b** Foliar treatment with AgNO_3 solution ($64 \mu\text{mol L}^{-1}$). As indicated, red, blue, and grey bars represent downregulated, upregulated, and genes that did not show statistical significance, respectively. '*' indicates gene expression statistical significance ($p < 0.05$)

Defensin-like (*DEFL*), Oxoglutarate-dependent dioxygenase (*DAO*), Fatty acid desaturase (*FADS*), and Pathogen-induced defense-responsive protein 8 (*PIDRP8*) genes were upregulated, while Stromal ascorbate peroxidase (*SAPX*) gene was downregulated, and the expression of Salt responsive protein 2 (*SRG2*), Avirulence-responsive family protein (*ARP*), and Cytochrome P450 (*CYP83B1*) genes did not exhibit statistically-significant modulation when compared to the mock-treated control condition. These results indicate that the application of AENFP-AgNPs at a concentration of $64 \mu\text{mol L}^{-1}$ triggers an effective defense response, probably due to the elicitor properties present in AgNPs synthesized from AENFP.

Plant leaves treated only with aqueous solution of AgNO_3 [$64 \mu\text{mol L}^{-1}$] also showed a modulatory effect on targeted genes, although to a lesser extent (Fig. 5b). The *DEFL* and *PIDRP8* genes were upregulated, while *SAPX* and *CYP83B1* genes were downregulated when compared to the control condition. These results suggest that the application of aqueous solution of AgNO_3 [$64 \mu\text{mol L}^{-1}$] in Brassica plants does not sufficiently trigger an effective defense response, although positive regulation of some genes was observed. The expression of the defense-related biomarker genes *FADS* and *DAO*, as well as the well-known pathogenesis-related (PR) genes *DEFL* and *PIDRP8* is reported to be induced during phytopathogen attack [71]. For example, the modulation of *FADS* gene expression has been shown to play an important role in plant resistance against various abiotic and biotic stressors, including cold, heat, drought, and pathogens [72–75]. On the other hand, the *DAO* gene converts the active IAA into biologically inactive 2-oxoindole-3-acetic acid (OxIAA), which is important in auxin catabolism and in maintaining central auxin homeostasis for reproductive development in plants [76]. Lastly, increased expression of both PR genes *DEFL* and *PIDRP8* has been associated with defense responses and developmental signaling in plants [77, 78]. The *SAPX* gene controls the content of hydrogen peroxide (H_2O_2) generated during abiotic and biotic stresses [79], while *CYP83B1* plays multiple roles in metabolic pathways and is essential for the biosynthesis of major phytoalexins (defense molecules) [80, 81].

Furthermore, the transcriptional modulation of other plant defense-related genes has been documented in studies involving AgNP treatments in crops. For instance, Noha, Bondok and El-DougDoug [82] showed that tomato plants, susceptible to Tomato mosaic virus (ToMV) and Potato virus Y (PVY), when treated with AgNPs showed positive alterations in the activity of peroxidase (*POD*) and polyphenol oxidase (*PPO*). Furthermore, studies carried out by Nair and Chung [83] demonstrated that mung bean (*Vigna radiata* L.) seedlings treated with AgNPs had the expression of superoxide dismutase (*SOD*), catalase (*CAT*), and ascorbate peroxidase (*APX*) defense-related genes positively modulated in comparison to the non-treated control plants.

Ultimately, although the complex molecular mechanisms underlying the defense response of *B. oleracea* elicited by AgNPs remain unclear, current gene expression analysis results, supported by literature, indicate that treating cabbage leaves with green-synthesized AENFP-AgNPs suspension triggers a plant defense response through effective modulation of defense-related genes. This finding highlights the potential of a nanobiotechnological approach for crop protection against black rot disease.

3.5 AENFP-AgNPs treated plants challenged with *Xcc* exhibited improved tolerance to black rot disease

To verify the potential of AENFP-AgNPs treatment to impair foliar tissue infection by *Xcc*, cabbage plant leaves were treated with AENFP-AgNPs and then inoculated with *Xcc* bacterial suspension at 24 h after application. The present results showed that the application of AENFP-AgNPs in cabbage plant leaves led to both a delay of typical black rot foliar symptoms and a significant reduction in the injured foliar area up to 7 dai (Fig. 6I, II). Foliar disease symptoms were first observed at 5 dai and were remarkably more pronounced in plants treated with AgNO_3 solution and in water mock-treated control conditions, where leaves exhibited prominent chlorotic spots and even necrotic areas (Fig. 6I). Black rot disease symptoms worsened by 7 dai, with leaves displaying a severely affected phenotype. The quantification of symptoms, expressed as the percentage of injured foliar area, showed that plants treated with AENFP-AgNPs exhibited a significantly lower percentage ($p\text{-value} < 0.05$) of damaged foliar area at 5 and 7 dai compared to the control condition (Fig. 6II). By the final time point (10 dai), a progressive normalization of symptoms was observed across all conditions, suggesting a loss of AgNPs functionality, likely due to the depletion of Ag^+ ions and/or the degradation or oxidation of bioactive compounds on the AgNPs surface. It is noteworthy that AgNO_3 treatment did not show statistically significant differences to the control group at any time point during the experimental assay. This finding further validates our results, which demonstrated that AENFP-AgNPs treatment primes defense responses in *B. oleracea* leaves and provides a temporary but remarkable protective effect against *Xcc*. This effect could perhaps be sustained with subsequent applications.

This study showed that the application of AENFP-AgNPs synthesized with 60 mg mL^{-1} of AENFP at a concentration at $64 \mu\text{mol L}^{-1}$ suppressed the development of black rot caused by *Xcc*, leading to increased protection. This protective effect is likely due to both direct interactions between AgNPs and *Xcc* cells and the elicitor properties of AENFP-AgNPs,

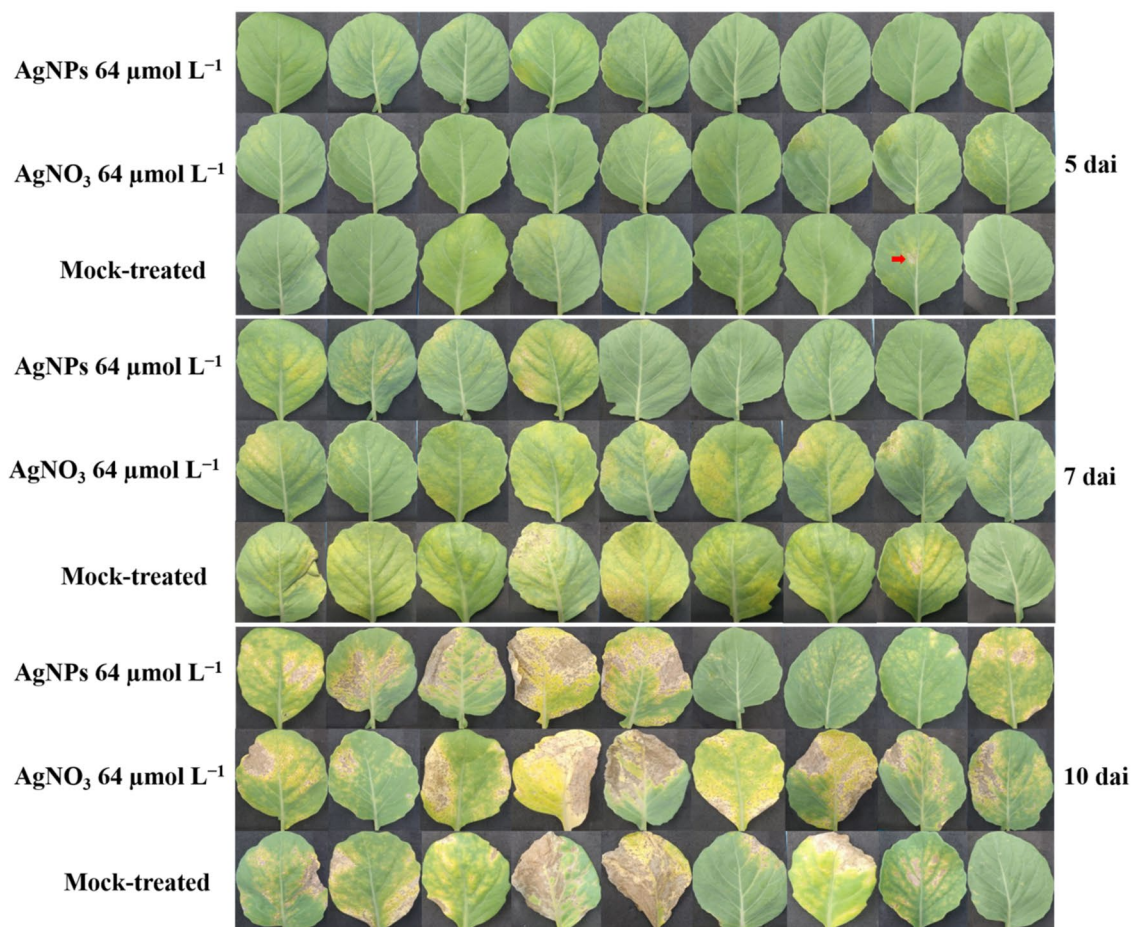
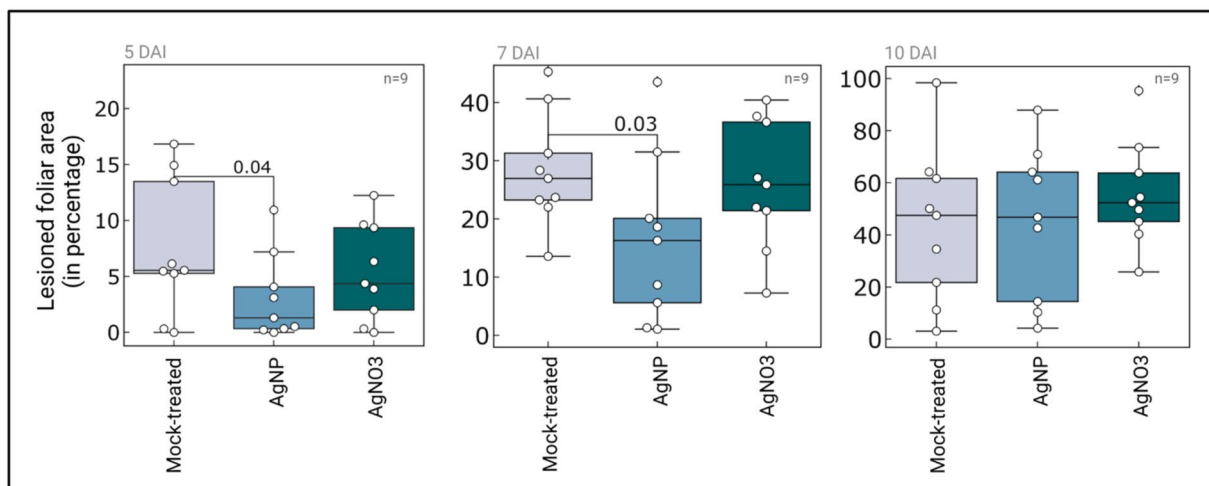
I**Leaves inoculated with *Xcc*****II**

Fig. 6 Challenging of AENFP-AgNPs treated cabbage plant leaves with *X. campestris* pv. *campestris* isolate *Xcc*51. **I** Black rot disease symptoms in cabbage leaves treated with AENFP-AgNPs synthesized with 60 mg mL⁻¹ of AENFP and 64 μmol L⁻¹ of silver nitrate (AgNO₃) solution (upper line), 64 μmol L⁻¹ of silver nitrate (AgNO₃) solution (middle line), and mock-treated water control condition (bottom line). The severity of symptoms was analyzed by using the software Quant[®] at three different time points 5, 7, and 10 days after inoculation (dai). The red arrow shows the damaged area in the mock-treated control conditions. **II** Significance for the ratio of the injured foliar area between treated and control groups was calculated by using one-way ANOVA ($p < 0.05$) followed by post hoc T-student test. Each colored boxplot represents the average (\pm SEM) of three biological replicates ($n = 9$ leaves)

which appear to induce systemic resistance. According to Ovais et al. [84], the main constituents of plant extracts include polyphenols (terpenoids, flavonoids, and tannins), proteins (enzymes), organic acids, and alkaloids, all of which can act as chemical agents to reduce silver ions and stabilize AgNPs. One of the most effective strategies for plant disease control has been the induction of host resistance [85]. Thus, the use of AENFP-AgNPs could also be extended to other crops to control different diseases and enhance overall productivity.

4 Conclusions

The results obtained in this study showed that the use of different aqueous extracts at different concentrations produced AgNPs with distinct characteristics, enabling their application for diverse purposes, such as the control of *Xcc* in Brassica crops. Furthermore, these results demonstrated that Brassica plants sprayed with AENFP-AgNPs synthesized with 60 mg mL⁻¹ of AENFP at a concentration of 64 µmol L⁻¹ induced systemic acquired resistance (SAR) against *Xcc*. This treatment activated the expression of specific defense-related genes, resulting in a significant reduction of disease symptoms and delaying disease progression. These findings suggest that AENFP-AgNPs function as elicitors of active defense responses in plants and exhibit effective antimicrobial activity against the phytopathogenic bacterium *Xcc*. Our study provides an alternative strategy for controlling black rot disease in cruciferous crops, reinforcing the potential of AgNPs in reducing the reliance on hazardous chemical pesticides. Such approaches align with the principles of environmental sustainability, balancing economic and ecological benefits to promote a more sustainable agricultural production.

Acknowledgements This study was financed in part by the Coordenação de Aperfeiçoamento de Pessoal de Nível Superior – Brasil (CAPES) – Finance Code 001, Embrapa, Conselho Nacional de Desenvolvimento Científico e Tecnológico – CNPq, and Fundação de Amparo Pesquisa do Distrito Federal – FAPDF. The authors have no conflict of interest to declare.

Author contributions All authors contributed to the study conception and design. Material preparation, data collection and analysis were performed by Ivonaldo Reis Santos, Fabiano Touzdzian Pinheiro Kohlrausch Távora, and Eduardo Andrade Franco Severo. Osmundo Oliveira-Neto assisted in plant cultivation and data analysis. Angela Mehta and Luciano Paulino Silva designed experiments, analyzed data, wrote the manuscript, and led the work. The first draft of the manuscript was written by Ivonaldo Reis Santos and all authors commented on previous versions of the manuscript. All authors read and approved the final manuscript.

Funding This study was financed in part by the Coordenação de Aperfeiçoamento de Pessoal de Nível Superior—Brasil (CAPES)—Finance Code 001, Embrapa, Conselho Nacional de Desenvolvimento Científico e Tecnológico—CNPq, and Fundação de Amparo Pesquisa do Distrito Federal—FAPDF.

Data availability The datasets generated during and/or analyzed during the current study are available from the corresponding author on reasonable request.

Declarations

Ethics approval and consent to participate The collection of the plants used in the study complies with local or national guidelines with no need for further affirmation.

Consent for publication The authors declare that this paper does not contain any studies with human participants or animals performed by any of the authors.

Competing interests The authors declare no competing interests.

Open Access This article is licensed under a Creative Commons Attribution-NonCommercial-NoDerivatives 4.0 International License, which permits any non-commercial use, sharing, distribution and reproduction in any medium or format, as long as you give appropriate credit to the original author(s) and the source, provide a link to the Creative Commons licence, and indicate if you modified the licensed material. You do not have permission under this licence to share adapted material derived from this article or parts of it. The images or other third party material in this article are included in the article's Creative Commons licence, unless indicated otherwise in a credit line to the material. If material is not included in the article's Creative Commons licence and your intended use is not permitted by statutory regulation or exceeds the permitted use, you will need to obtain permission directly from the copyright holder. To view a copy of this licence, visit <http://creativecommons.org/licenses/by-nc-nd/4.0/>.

References

1. Warwick S, Francis A, Al-Shehbaz I. Brassicaceae: species checklist and database on CD-Rom. *Plant Syst Evol.* 2006;259(2):249–58. <https://doi.org/10.1007/s00606-006-0422-0>.
2. Hafidh R, Abdulamir A, Bakar FA, Jalilian F, Jahanshahi F, Abas F, Sekawi Z. Novel anticancer activity and anticancer mechanisms of *Brassica oleracea* L. var. *capitata* f. *rubra*. *Eur J Integr Med.* 2013;5(5):450–64. <https://doi.org/10.1016/j.eujim.2013.06.004>.
3. Zielińska M, Lewandowska U, Podśędek A, Cygankiewicz AI, Jacenik D, Sałaga M, Kordek R, Krajewska WM, Fichna J. Orally available extract from *Brassica oleracea* var. *capitata* rubra attenuates experimental colitis in mouse models of inflammatory bowel diseases. *J Funct Foods.* 2015;17:587–99. <https://doi.org/10.1016/j.jff.2015.05.046>.
4. Liu S, Liu Y, Yang X, Tong C, Edwards D, Parkin IA, Zhao M, Ma J, Yu J, Huang S. The *Brassica oleracea* genome reveals the asymmetrical evolution of polyploid genomes. *Nat Commun.* 2014;5(1):1–11. <https://doi.org/10.1038/ncomms4930>.
5. Griesbach E, Löptien H, Miersch U. Resistenz gegen *Xanthomonas campestris* pv. *campestris* (Pammel) Dowson im Kohl *Brassica oleracea* L. *JPDP.* 2003;110:461–75. <https://doi.org/10.1007/BF03356123>.
6. Santos LS, Maximiano MR, Megias E, Pappas M, Ribeiro SG, Mehta A. Quantitative expression of microRNAs in *Brassica oleracea* infected with *Xanthomonas campestris* pv. *campestris*. *Mol Biol Rep.* 2019;46(3):3523–9. <https://doi.org/10.1007/s11033-019-04779-7>.
7. Mishra S, Arora NK. Management of black rot in cabbage by rhizospheric *Pseudomonas* species and analysis of 2, 4-diacetylphloroglucinol by qRT-PCR. *Biocontrol.* 2012;61(1):32–9. <https://doi.org/10.1016/j.biocontrol.2011.12.011>.
8. Aires A, Dias CS, Carvalho R, Oliveira MH, Monteiro AA, Simões MV, Rosa EA, Bennett RN, Saavedra MJ. Correlations between disease severity, glucosinolate profiles and total phenolics and *Xanthomonas campestris* pv. *campestris* inoculation of different Brassicaceae. *Sci Hortic.* 2011;129(3):503–10. <https://doi.org/10.1016/j.scienta.2011.04.009>.
9. Vicente JG, Holub EB. *Xanthomonas campestris* pv. *campestris* (cause of black rot of crucifers) in the genomic era is still a worldwide threat to brassica crops. *Mol Plant Pathol.* 2013;14(1):2–18. <https://doi.org/10.1111/j.1364-3703.2012.00833.x>.
10. Dow JM, Crossman L, Findlay K, He Y-Q, Feng J-X, Tang J-L. Biofilm dispersal in *Xanthomonas campestris* is controlled by cell-cell signaling and is required for full virulence to plants. *PNAS.* 2003;100(19):10995–1000. <https://doi.org/10.1073/pnas.1833360100>.
11. Taylor J, Conway J, Roberts S, Astley D, Vicente J. Sources and origin of resistance to *Xanthomonas campestris* pv. *campestris* in Brassica genomes. *Phytopathology.* 2002;92(1):105–11. <https://doi.org/10.1094/PHYTO.2002.92.1.105>.
12. Kumar A, Choudhary A, Kaur H, Guha S, Mehta S, Husen A. Potential applications of engineered nanoparticles in plant disease management: a critical update. *Chemosphere.* 2022;295:133798. <https://doi.org/10.1016/j.chemosphere.2022.133798>.
13. Badawy AA, Husen A, Salem SS. Use of nanobiotechnology in augmenting soil–plant system interaction for higher plant growth and production, Essential minerals in plant-soil systems. Amsterdam: Elsevier; 2024. p. 423–43.
14. Abdelfattah NA, Yousef MA, Badawy AA, Salem SS. Influence of biosynthesized magnesium oxide nanoparticles on growth and physiological aspects of cowpea (*Vigna unguiculata* L.) plant, cowpea beetle, and cytotoxicity. *Biotechnol J.* 2023;18(12):2300301. <https://doi.org/10.1002/biot.202300301>.
15. Guo T, Yao M-S, Lin Y-H, Nan C-W. A comprehensive review on synthesis methods for transition-metal oxide nanostructures. *Cryst-EngComm.* 2015;17(19):3551–85. <https://doi.org/10.1039/C5CE00034C>.
16. Das P, Ghosal K, Jana NK, Mukherjee A, Basak P. Green synthesis and characterization of silver nanoparticles using belladonna mother tincture and its efficacy as a potential antibacterial agent. *Mater Chem Phys.* 2019;228:310–7. <https://doi.org/10.1016/j.matchemphys.2019.02.064>.
17. Ahmad S, Munir S, Zeb N, Ullah A, Khan B, Ali J, Bilal M, Omer M, Alamzeb M, Salman SM. Green nanotechnology: a review on green synthesis of silver nanoparticles—an ecofriendly approach. *Int J Nanomed.* 2019;14:5087. <https://doi.org/10.2147/IJN.S200254>.
18. Amin MA, Ismail MA, Badawy AA, Awad MA, Hamza MF, Awad MF, Fouda A. The Potency of fungal-fabricated selenium nanoparticles to improve the growth performance of *Helianthus annuus* L. and control of cutworm *Agrotis ipsilon*. *Catalysts.* 2021;11(12):1551. <https://doi.org/10.3390/catal11121551>.
19. Badawy AA, Abdelfattah NA, Salem SS, Awad MF, Fouda A. Efficacy assessment of biosynthesized copper oxide nanoparticles (CuO-NPs) on stored grain insects and their impacts on morphological and physiological traits of wheat (*Triticum aestivum* L.) plant. *Biology.* 2021;10(3):233. <https://doi.org/10.3390/biology10030233>.
20. Guan Z, Ying S, Ofoegbu PC, Clubb P, Rico C, He F, Hong J. Green synthesis of nanoparticles: current developments and limitations. *Environ Technol Innov.* 2022. <https://doi.org/10.1016/j.eti.2022.102336>.
21. Ahmed S, Ahmad M, Swami BL, Ikram S. A review on plants extract mediated synthesis of silver nanoparticles for antimicrobial applications: a green expertise. *J Adv Res.* 2016;7(1):17–28. <https://doi.org/10.1016/j.jare.2015.02.007>.
22. Rafique M, Sadaf I, Rafique MS, Tahir MB. A review on green synthesis of silver nanoparticles and their applications, artificial cells, nanomedicine, and *Artif. Cells Nanomed Biotechnol.* 2017;45(7):1272–91. <https://doi.org/10.1080/21691401.2016.1241792>.
23. Mohapatra B, Kuriakose S, Mohapatra S. Rapid green synthesis of silver nanoparticles and nanorods using *Piper nigrum* extract. *J Alloys Compd.* 2015;637:119–26. <https://doi.org/10.1016/j.jallcom.2015.02.206>.
24. Sekhon BS. Nanotechnology in agri-food production: an overview. *Nanotechnol Sci Appl.* 2014. <https://doi.org/10.2147/NSA.S39406>.
25. Thiruvengadam M, Rajakumar G, Chung I-M. Nanotechnology: current uses and future applications in the food industry. *3 Biotech.* 2018;8:1–13. <https://doi.org/10.1007/s13205-018-1104-7>.
26. Rehman S, Jermy R, Asiri SM, Shah MA, Farooq R, Ravinayagam V, Ansari MA, Alsalem Z, Al Jindan R, Reshi Z. Using *Fomitopsis pinicola* for bioinspired synthesis of titanium dioxide and silver nanoparticles, targeting biomedical applications. *RSC Adv.* 2020;10(53):32137–47. <https://doi.org/10.1039/D0RA02637A>.
27. Chung I-M, Park I, Seung-Hyun K, Thiruvengadam M, Rajakumar G. Plant-mediated synthesis of silver nanoparticles: their characteristic properties and therapeutic applications. *Nanoscale Res Lett.* 2016;11(1):1–14. <https://doi.org/10.1186/s11671-016-1257-4>.
28. Moodley JS, Krishna SBN, Pillay K, Govender P. Green synthesis of silver nanoparticles from *Moringa oleifera* leaf extracts and its antimicrobial potential. *Adv Nat Sci J Nanosci Nanotechnol.* 2018;9(1):015011. <https://doi.org/10.1088/2043-6254/aaabb2>.

29. Santiago TR, Bonatto CC, Rossato M, Lopes CA, Lopes CA, Mizubuti ESG, Silva LP. Green synthesis of silver nanoparticles using tomato leaf extract and their entrapment in chitosan nanoparticles to control bacterial wilt. *J Sci Food Agric*. 2019;99(9):4248–59. <https://doi.org/10.1002/jsfa.9656>.
30. Sambrook J, Fritsch EF, Maniatis T. Molecular cloning: a laboratory manual. New York: Cold spring harbor laboratory press; 1989.
31. Santos IR, Ribeiro DG, Távora FTPK, Maximiano MR, Rabelo AC, Rios TB, Reis Junior FB, Megías M, Silva LP, Mehta A. Priming of defense-related genes in *Brassica oleracea* var. *capitata* using concentrated metabolites produced by *Rhizobium tropici* CIAT 899. *Braz J Microbiol*. 2022. <https://doi.org/10.1007/s42770-022-00722-4>.
32. Untergasser A, Cutcutache I, Koressaar T, Ye J, Faircloth BC, Remm M, Rozen SG. Primer3—new capabilities and interfaces. *Nucleic Acids Res*. 2012;40(15):e115–e115. <https://doi.org/10.1093/nar/gks596>.
33. Owczarzy R, Tataurov AV, Wu Y, Manthey JA, McQuisten KA, Almabrazi HG, Pedersen KF, Lin Y, Garretson J, McEntaggart NO. IDT SciTools: a suite for analysis and design of nucleic acid oligomers. *Nucleic Acids Res*. 2008;36:W163–9. <https://doi.org/10.1093/nar/gkn198>.
34. Santos IR, Maximiano MR, Almeida RF, da Cunha RNV, Lopes R, Scherwinski-Pereira JE, Mehta A. Genotype-dependent changes of gene expression during somatic embryogenesis in oil palm hybrids (*Elaeis oleifera* x *E. guineensis*). *Plos ONE*. 2018;13(12):e0209445. <https://doi.org/10.1371/journal.pone.0209445>.
35. Zhao S, Fernald RD. Comprehensive algorithm for quantitative real-time polymerase chain reaction. *J Comput Biol*. 2005;12(8):1047–64. <https://doi.org/10.1089/cmb.2005.12.1047>.
36. Pfaffl MW, Horgan GW, Dempfle L. Relative expression software tool (REST©) for group-wise comparison and statistical analysis of relative expression results in real-time PCR. *Nucleic Acids Res*. 2002;30(9):e36–e36. <https://doi.org/10.1093/nar/30.9.e36>.
37. Guénin S, Mauriat M, Pelloux J, Van Wuytswinkel O, Bellini C, Gutierrez L. Normalization of qRT-PCR data: the necessity of adopting a systematic, experimental conditions-specific, validation of references. *J Exp Bot*. 2009;60(2):487–93. <https://doi.org/10.1093/jxb/ern305>.
38. Vale F, Fernandes Filho E, Liberato J, QUANT. A software for plant disease severity assessment, 8th international congress of plant pathology, Christchurch New Zealand. 2003; 105.
39. Baker S, Rakshith D, Kavitha KS, Santosh P, Kavitha HU, Rao Y, Satish S. Plants: emerging as nanofactories towards facile route in synthesis of nanoparticles. *Biol Impacts: BI*. 2013;3(3):111. <https://doi.org/10.5681/bi.2013.012>.
40. Sytu MRC, Camacho DH. Green synthesis of silver nanoparticles (AgNPs) from *Lenzites betulina* and the potential synergistic effect of AgNP and capping biomolecules in enhancing antioxidant activity. *BioNanoScience*. 2018;8:835–44. <https://doi.org/10.1007/s12668-018-0548-x>.
41. Alsammarie FK, Wang W, Zhou P, Mustapha A, Lin M. Green synthesis of silver nanoparticles using turmeric extracts and investigation of their. *Colloids Surf, B*. 2018;171:398–405. <https://doi.org/10.1016/j.colsurfb.2018.07.059>.
42. Ahmed S, Ahmad M, Swami BL, Ikram S. Green synthesis of silver nanoparticles using *Azadirachta indica* aqueous leaf extract. *J Radiat Res Appl Sci*. 2016;9(1):1–7. <https://doi.org/10.4172/2157-7439.1000452>.
43. Vuanghao L, Laghari M. *Morinda citrifolia* (Noni): a comprehensive review on its industrial uses, pharmacological activities, and clinical trials. *Arab J Chem*. 2017;10:691–707. <https://doi.org/10.1016/j.arabjc.2015.06.018>.
44. Singh D. *Morinda citrifolia* L.(Noni): a review of the scientific validation for its nutritional and therapeutic properties. *JDE*. 2012;3(6):77–91.
45. Feng QL, Wu J, Chen GQ, Cui F, Kim T, Kim J. A mechanistic study of the antibacterial effect of silver ions on *Escherichia coli* and *Staphylococcus aureus*. *J J Biomed Mater Res*. 2000;52(4):662–8. [https://doi.org/10.1002/1097-4636\(20001215\)52:4%3c662::AID-JBM10%3e3.0.CO;2-3](https://doi.org/10.1002/1097-4636(20001215)52:4%3c662::AID-JBM10%3e3.0.CO;2-3).
46. Dorobantu LS, Fallone C, Noble AJ, Veinot J, Ma G, Goss GG, Burrell RE. Toxicity of silver nanoparticles against bacteria, yeast, and algae. *J Nanoparticle Res*. 2015;17(4):1–13. <https://doi.org/10.1007/s11051-015-2984-7>.
47. Ferdous Z, Nemmar A. Health impact of silver nanoparticles: a review of the biodistribution and toxicity following various routes of exposure. *Int J Mol Sci*. 2020;21(7):2375. <https://doi.org/10.3390/ijms21072375>.
48. Martinez-Gutierrez F, Olive PL, Banuelos A, Orrantia E, Nino N, Sanchez EM, Ruiz F, Bach H, Av-Gay Y. Synthesis, characterization, and evaluation of antimicrobial and cytotoxic effect of silver and titanium nanoparticles. *Nanomed Nanotechnol Biol Med*. 2010;6(5):681–8. <https://doi.org/10.1016/j.nano.2010.02.001>.
49. Ivask A, ElBadawy A, Kaweeteerawat C, Boren D, Fischer H, Ji Z, Chang CH, Liu R, Tolaymat T, Telesca D. Toxicity mechanisms in *Escherichia coli* vary for silver nanoparticles and differ from ionic silver. *ACS Nano*. 2014;8(1):374–86. <https://doi.org/10.1021/nn4044047>.
50. Pérez-Díaz MA, Boegli L, James G, Velasquillo C, Sanchez-Sanchez R, Martinez-Martinez R-E, Martínez-Castañón GA, Martínez-Gutierrez F. Silver nanoparticles with antimicrobial activities against *Streptococcus mutans* and their cytotoxic effect. *Mater Sci Eng C*. 2015;55:360–6. <https://doi.org/10.1016/j.msec.2015.05.036>.
51. Karakoti A, Hench L, Seal S. The potential toxicity of nanomaterials—the role of surfaces. *Jom*. 2006;58(7):77–82. <https://doi.org/10.1007/s11837-006-0147-0>.
52. Kumar R, Ghoshal G, Jain A, Goyal M. Rapid green synthesis of silver nanoparticles (AgNPs) using (*Prunus persica*) plants extract: exploring its antimicrobial and catalytic activities. *J Nanomed Nanotechnol*. 2017;8(4):1–8. <https://doi.org/10.4172/2157-7439.1000452>.
53. Awwad AM, Salem NM. Green synthesis of silver nanoparticles by Mulberry Leaves Extract. *Nanosci Nanotechnol*. 2012;2(4):125–8.
54. Ahmad N, Sharma S. Green synthesis of silver nanoparticles using extracts of *Ananas comosus*. *Green Sustain Chem*. 2012. <https://doi.org/10.4236/gsc.2012.24020>.
55. Carson L, Bandara S, Joseph M, Green T, Grady T, Osuji G, Weerasooriya A, Ampim P, Woldesenbet S. Green synthesis of silver nanoparticles with antimicrobial properties using *Phyla dulcis* plant extract. *Foodborne Pathog Dis*. 2020;17(8):504–11. <https://doi.org/10.1089/fpd.2019.2714>.
56. Pupe JM, Silva LP. Modulation of physico-chemical and biological properties of silver nanoparticles synthesized using aqueous extract of flamboyant (*Delonix regia* var. *flavida*, *Fabaceae*) seeds. *J Clust Sci*. 2021;32(4):1053–60. <https://doi.org/10.1007/s10876-020-01871-y>.
57. Vijayakumar S, Divya M, Vaseeharan B, Chen J, Biruntha M, Silva LP, Durán-Lara EF, Shreema K, Ranjan S, Dasgupta N. Biological compound capping of silver nanoparticle with the seed extracts of blackcumin (*Nigella sativa*): a potential antibacterial, antidiabetic, anti-inflammatory, and antioxidant. *J J Inorg Organomet Polym Mater*. 2021;31(2):624–35. <https://doi.org/10.1007/s10904-020-01713-4>.
58. Pereira TM, Polez VLP, Sousa MH, Silva LP. Modulating physical, chemical, and biological properties of silver nanoparticles obtained by green synthesis using different parts of the tree *Handroanthus heptaphyllus* (Vell.) Mattos. *Colloids Interface Sci Commun*. 2020;34:100224. <https://doi.org/10.1016/j.colcom.2019.100224>.

59. Savithramma N, Linga Rao M, Ankanna S, Venkateswarlu P. Screening of medicinal plants for effective biogenesis of silver nanoparticles and efficient antimicrobial activity. *Int J Pharm Sci.* 2012;3(4):1141–8.
60. Lee HY, Park HK, Lee YM, Kim K, Park SB. A practical procedure for producing silver nanocoated fabric and its antibacterial evaluation for biomedical applications. *Chem Commun.* 2007. <https://doi.org/10.1039/b703034g>.
61. El Badawy AM, Silva RG, Morris B, Scheckel KG, Suidan MT, Tolaymat TM. Surface charge-dependent toxicity of silver nanoparticles. *Environ Sci Technol.* 2011;45(1):283–7. <https://doi.org/10.1021/es1034188>.
62. Sohm B, Immel F, Bauda P, Pagnout C. Insight into the primary mode of action of TiO₂ nanoparticles on *Escherichia coli* in the dark. *Proteomics.* 2015;15(1):98–113. <https://doi.org/10.1002/pmic.201400101>.
63. Abdou E, Abd-Alla H, Galal A. Survey of sesame root rot/wilt disease in Minia and their possible control by ascorbic salicylic acids, AJAS (Egypt). 2003. <https://doi.org/10.5555/20013166158>
64. Elsharkawy M, Shimizu M, Takahashi H, Hyakumachi M. Induction of systemic resistance against Cucumber mosaic virus by *Penicillium simplicissimum* GP17-2 in *Arabidopsis* and tobacco. *Plant Pathol.* 2012;61(5):964–76. <https://doi.org/10.1111/j.1365-3059.2011.02573.x>.
65. Kanhed P, Birla S, Gaikwad S, Gade A, Seabra AB, Rubilar O, Duran N, Rai M. In vitro antifungal efficacy of copper nanoparticles against selected crop pathogenic fungi. *Mater Lett.* 2014;115:13–7. <https://doi.org/10.1016/j.matlet.2013.10.011>.
66. Abdelmoteleb A, Gonzalez-Mendoza D, Valdez-Salas B, Grimaldo-Juarez O, Ceceña-Duran C. Inhibition of Fusarium solani in transgenic insect-resistant cotton plants treated with silver nanoparticles from *Prosopis glandulosa* and *Pluchea sericea*. *Egypt J Biol Pest Control.* 2018;28(1):1–5. <https://doi.org/10.1186/s41938-017-0005-0>.
67. Elsharkawy MM, Derbalah A. Antiviral activity of titanium dioxide nanostructures as a control strategy for broad bean strain virus in faba bean. *Pest Manag Sci.* 2019;75(3):828–34. <https://doi.org/10.1002/ps.5185>.
68. Kumar V, Yadav SK. Plant-mediated synthesis of silver and gold nanoparticles and their applications. *J Chem Technol Biotechnol Int Res Process Environ Clean Technol.* 2009;84(2):151–7. <https://doi.org/10.1002/jctb.2023>.
69. Morsy MK, Elsbagh R, Trinetta V. Evaluation of novel synergistic antimicrobial activity of nisin, lysozyme, EDTA nanoparticles, and/or ZnO nanoparticles to control foodborne pathogens on minced beef. *Food Control.* 2018;92:249–54. <https://doi.org/10.1016/j.foodcont.2018.04.061>.
70. Alam T, Khan RAA, Ali A, Sher H, Ullah Z, Ali M. Biogenic synthesis of iron oxide nanoparticles via *Skimmia laureola* and their antibacterial efficacy against bacterial wilt pathogen *Ralstonia solanacearum*. *Mater Sci Eng.* 2019;98:101–8. <https://doi.org/10.1016/j.msec.2018.12.117>.
71. Jiang H, Song W, Li A, Yang X, Sun D. Identification of genes differentially expressed in cauliflower associated with resistance to *Xanthomonas campestris* pv. *campestris*. *Mol Biol Rep.* 2011;38(1):621–9. <https://doi.org/10.1007/s11033-010-0148-5>.
72. Celik Altunoglu Y, Unel NM, Baloglu MC, Ulu F, Can TH, Cetinkaya R. Comparative identification and evolutionary relationship of fatty acid desaturase (FAD) genes in some oil crops: the sunflower model for evaluation of gene expression pattern under drought stress. *Biotechnol Biotechnol Equip.* 2018;32(4):846–57. <https://doi.org/10.1080/13102818.2018.1480421>.
73. Xu L, Zeng W, Li J, Liu H, Yan G, Si P, Yang C, Shi Y, He Q, Zhou W. Characteristics of membrane-bound fatty acid desaturase (FAD) genes in *Brassica napus* L. and their expressions under different cadmium and salinity stresses. *Environ Exp Bot.* 2019;162:144–56. <https://doi.org/10.1016/j.envexpbot.2019.02.016>.
74. Xue Y, Zhang X, Wang R, Chen B, Jiang J, Win AN, Chai Y. Cloning and expression of *Perilla frutescens* FAD2 gene and polymorphism analysis among cultivars. *Acta Physiol Plant.* 2017;39(3):84. <https://doi.org/10.1016/j.envexpbot.2019.02.016>.
75. Cao Z, Rosenkranz D, Wu S, Liu H, Pang Q, Zhang X, Liu B, Zhao B. Different classes of small RNAs are essential for head regeneration in the planarian *Dugesia japonica*. *BMC genomic.* 2020;21(1):1–11. <https://doi.org/10.1186/s12864-020-07234-1>.
76. Zhao Z, Zhang Y, Liu X, Zhang X, Liu S, Yu X, Ren Y, Zheng X, Zhou K, Jiang L. A role for a dioxygenase in auxin metabolism and reproductive development in rice. *Dev Cell.* 2013;27(1):113–22. <https://doi.org/10.1016/j.devcel.2013.09.005>.
77. Xiong M, Wang S, Zhang Q. Coincidence in map positions between pathogen-induced defense-responsive genes and quantitative resistance loci in rice, science China. *Life Sci.* 2002;5(5):518–26. <https://doi.org/10.1360/02yc9057>.
78. Dresselhaus T, Márton ML. Micropylar pollen tube guidance and burst: adapted from defense mechanisms? *Curr Opin Plant Biol.* 2009;12(6):773–80. <https://doi.org/10.1016/j.pbi.2009.09.015>.
79. Maruta T, Ishikawa T. Ascorbate peroxidase functions in higher plants: the control of the balance between oxidative damage and signaling. In: Gupta DK, Palma JM, Corpas FJ, editors. *Antioxidants and antioxidant enzymes in higher plants*. Cham: Springer; 2018. p. 41–59. https://doi.org/10.1007/978-3-319-75088-0_3
80. Durst F, Benveniste I. Cytochrome P450 in plants, cytochrome P450. Berlin: Springer; 1993. p. 293–310.
81. Xu J, Wang X, Guo W. The cytochrome P450 superfamily: key players in plant development and defense. *J Integr Agric.* 2015;14:1673–86. [https://doi.org/10.1016/S2095-3119\(14\)60980-1](https://doi.org/10.1016/S2095-3119(14)60980-1).
82. Noha K, Bondok A, El-Dougoudou K. Evaluation of silver nanoparticles as antiviral agent against ToMV and PVY in tomato plants. *Sciences.* 2018;8(01):100–11.
83. Nair PMG, Chung IM. Physiological and molecular level studies on the toxicity of silver nanoparticles in germinating seedlings of mung bean (*Vigna radiata* L.). *Acta Physiol Plant.* 2015;1:1–11. <https://doi.org/10.1007/s11738-014-1719-1>.
84. Ovais M, Khalil AT, Islam NU, Ahmad I, Ayaz M, Saravanan M, Shinwari ZK, Mukherjee S. Role of plant phytochemicals and microbial enzymes in biosynthesis of metallic nanoparticles. *Appl Microbiol Biotechnol.* 2018;102(16):6799–814. <https://doi.org/10.1007/s00253-018-9146-7>.
85. Servin A, Elmer W, Mukherjee A, la Torre-Roche D, Hamdi H, White JC, Bindraban P, Dimkpa C. A review of the use of engineered nanomaterials to suppress plant disease and enhance crop yield. *J Nanoparticle Res.* 2015;17(2):1–21. <https://doi.org/10.1007/s11051-015-2907-7>.